Advances in Technology Innovation, vol. x, no. x, 20xx, pp. xx-xx

# Flow Separation Characteristics of Tandem Minibus Model Configuration

Melkiyanto, Nasaruddin Salam*, Rustan Tarakka

Department of Mechanical Engineering, Faculty of Engineering, Hasanuddin University, Gowa, Indonesia

Received 29 June 2024; received in revised form 21 November 2024; accepted 26 November 2024

DOI: https://doi.org/10.46604/aiti.2024.13942

## Abstract

This study aims to determine the characteristics of the pressure coefficient and fluid flow separation in a tandem minibus model using the Fluent 6.3.26 computational method and experimental testing in a wind tunnel. Pressure measurements are taken by installing 14 pressure taps connected to a manometer on a 1:40-scale minibus model. Tests were conducted at five different distances between minibuses in a series configuration at seven-speed levels. The results showed that at the highest speed tested, minimal flow separation occurred at a distance ratio of $L/D$ = 0.455, with values of $C_P$ = -0.083 in the first minibus and $C_P$ = -0.250 in the second minibus. This configuration is identified as the optimal spacing to reduce aerodynamic disturbance in the tandem minibus system.

**Keywords:** pressure coefficient, flow separation, tandem minibus configuration, computational fluid dynamics (CFD), fluent software

## 1. Introduction

In the design field, especially for vehicles and infrastructure, such as buildings and utilities, understanding the characteristics of aerodynamic flow is crucial for achieving optimal form and adequate strength, particularly when facing wind loads. Wind strength becomes a crucial factor that must be considered to ensure effective and efficient object functionality. In reducing energy losses and delaying the occurrence of flow separation when fluid passes through an object, it must be a primary factor in designing both the shape and structure to generate a uniform flow that provides significant advantages to the overall performance of the object [1-2].

Speed greatly affects the drag force. As the speed increases, the drag force value will increase, and the drag coefficient will decrease. The addition of deflectors can reduce fuel consumption on trucks at a speed of 100 km/h, producing a drag force of 394,768 N with a value of $C_D$ = 0.743 [2].

Positioning models in tandem affect flow field characteristics and delay flow separation [3–5]. For two tandem objects with varying diameters, at $Re$ = 3900 and $L/D$ = 1.00–1.50, the flow shows small-scale periodic reattachment [6]. Tandem body configurations have been widely studied experimentally and computationally [7]. Research on tandem circular cylinders reveals that at a relative roughness height of $\varepsilon/D$ = 0.001, the Strouhal number decreases by 6.25%, and drag on the upstream cylinder is reduced by 16.42% [8].

Two tandem cylinders with varying Reynolds numbers and spacing ($L/D$) were studied experimentally in a low-speed wind tunnel. At $L/D$ = 1.8, stable shear layer reattachment was observed, enhancing the understanding of airflow around tandem cylinders [9]. For triangular and square cylinders, increasing $L/D$ shifts the vortex toward the triangular cylinder,

* Corresponding author. E-mail address: nassalam.unhas@yahoo.co.id

English language proofreader: Si-Yu Lin

raising drag coefficients [10]. Square cylinders of equal size, tested at Reynolds numbers (*Re*) from 1 to 200 with $G = 5$ (where G is the gap or spacing between the two cylinders), showed steady flow at $Re \leq 35$ and unsteady flow at $Re \geq 40$ [11].

The geometry and spacing of test objects in tandem influence fluid flow behavior [12–13]. For a rectangular cylinder, increasing aspect ratios (*AR*) reduces drag force by 65% upstream, with a gap spacing of (G = 4) for $AR = 1$ [14]. Large eddy simulations of square cylinders under extreme wind pressure reveal that gap and wall vortices significantly impact extreme pressure, while corner vortices drive negative pressure near the upstream cylinder's front corner and the rear corners of both cylinders [15].

The spacing between three tandem cars significantly reduces drag and lift coefficients, with the lowest drag values corresponding to reduced lift coefficients [16]. For tandem square cylinders, vibration phenomena occur at low Reynolds numbers, but a vibration control device suppresses vibrations by 98% and 97% at $Re = 100$ [17]. Using splitter plates on tandem square cylinders with *G/D* variations reduces resistance by 1.61% for the upstream and 7.26% for the downstream cylinder at $G/D = 4$ [18]. Spacing and diameter of tandem airfoils greatly influence fluid flow, with experimental results showing flow separation near the trailing edge can be eliminated at 8°–10° and delayed at angles >10° [19, 20].

For tandem minibus models in four configurations, increasing speed and decreasing distance minimize drag, with the lowest drag coefficient (0.78) observed in configuration III [12]. By varying specimen spacing and adding a disturbance body, experimental and computational analysis shows the lowest drag coefficient (1.67) and pressure coefficient (0.87) at $L/D = 0.43$ and $d/D = 0.14$ (where d/D represents the ratio of the disturbance body inlet cylinder diameter to the square cylinder diameter), with reductions of 21.6% and 14.7%, respectively [21]. CFD simulations of three tandem minibuses arranged in four configurations at 20 m/s reveal that configuration III achieves the best pressure coefficient at $L/D = 2.75$ and $M/D = 0.57$ (where M/D represents the ratio of the distance in the Y direction (M) to the diameter of the minibus model) [1].

The spacing ratio in the configuration of three cylinders arranged in tandem, with a range of $L/D = 2$ to 6 at $Re = 150$, has a significant effect on the aerodynamic drag of the test model. This study shows that the distance between cylinders in a tandem configuration greatly affects the aerodynamic characteristics, where the secondary vortices in the wake area exhibit higher energy, and the center cylinder experiences negative drag at a small distance. Based on the results, the best spacing for this configuration is $L/D = 2$, which is the most optimal spacing compared to other *L/D* variations [22].

A 2D simulation studied flow past twin tandem rectangular cylinders at $Re = 150$, varying gap ratios ($L^*$ = cylinder spacing normalized by length, 1.0–8.0) and aspect ratios ($B^*$ = width-to-height ratio, 0.3–4.0). Fluid force trends categorized gaps as narrow ($L^* = 1.0–2.0$), medium ($L^* = 3.0–4.0$), and wide ($L^* = 6.0–8.0$). Higher $B^*$ reduced downstream cylinder (DC) force fluctuations for narrow gaps but amplified them for wide gaps. Wake flow showed a 2S vortex pattern (two single vortices) for narrow gaps and shifted from synchronized C(2S) to 2S for medium and wide gaps as $B^*$ increased. Proper orthogonal decomposition revealed the mechanisms behind these fluid force and vortex changes [23].

The drag coefficient, which measures the aerodynamic resistance experienced by a minibus, has been determined at 0.4 through rigorous testing and analysis, indicating the vehicle's capability to navigate the airflow with relative ease and efficiency. However, to achieve the optimal coefficient of pressure ($C_P$) value and delay flow separation, the minibusses are arranged into a tandem formation by varying the distance between them [1, 24].

Based on the theory and research results that have been presented, the distance between tandem objects in a series configuration significantly influences the pressure distribution and aerodynamic resistance experienced by each model. Therefore, this study aims to determine the distance between the minibus that yields the optimal coefficient of pressure ($C_P$). In addition, this study also seeks to characterize the flow separation on the surface of the minibus arranged in tandem series both experimentally and computationally using Fluent 6.3.26 software. To answer these problems, the following sections present the results of research and analysis of the characteristics of these variables.

## 2. Methodology

The minibus as the specimen of this research employs two methods: the first method is experimental, conducted in a subsonic wind tunnel, and the second method is computational fluid dynamics (CFD) applied using the Fluent 6.3.26 software to simulate the series tandem minibus model. Meanwhile, the dimensions of the test object use two minibus vehicle models with the following specifications: They are made of iron with a thickness of 1 mm and a length of 121 mm. The width of the minibus is 45 mm, the height is 43 mm, and the hydraulic diameter ($D$) has a value of 44 mm, with an actual scale ratio of 1: 40.

The two minibuses are arranged in a tandem series configuration with five levels of distance variation ($L$) of 10, 20, 30, 40, and 50 mm. Seven levels of variation in the same upstream speed starting from ($U$) = 8, 10, 12, 14, 16, 18, and 20 m/s.

For this reason, in this study, where Fig. 1 describes the position of the first and second minibus arranged in a series tandem configuration, which is given a treatment of variation in the ratio of distance and diameter ($L/D$) of five levels of variation, namely at $L/D$ = 0.227, 0.455, 0.682, 0.909, and 1.136.


Fig. 1 The positions of the first minibus and the second minibus in a series tandem model

Furthermore, Fig. 2 illustrates the position of each pressure tap installed around the body of the first minibus and the second minibus arranged in a tandem series configuration. Each minibus is fitted with 14 pressure taps: 3 pressure taps at the front, 3 at the rear, 4 on the left side, and 4 on the right side of the minibus body. These taps are useful for measuring the pressure distribution around the test model body connected directly to the manometer.

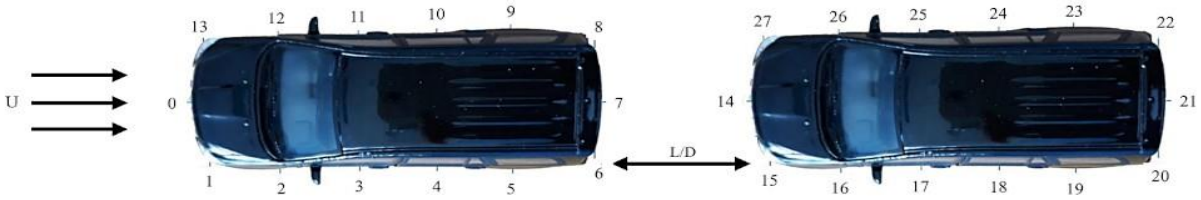


Fig. 2 Position of each pressure tap for the series configuration

The Reynolds number equation provided is used to analyze and determine the flow characteristics passing through the tandem minibus configuration and is expressed as

$$Re = \frac{U \cdot D}{\upsilon} \tag{1}$$

In Eq. (1), the variables and parameters involved include the upstream velocity ($U$), minibus model hydraulic diameter ($D$), and fluid kinematic viscosity ($\upsilon$).

To calculate the diameter of the minibus, the following equation can be used:

$$D = \frac{4 \cdot A}{p} \tag{2}$$

The variables and parameters presented in Eq. (2) include frontal cross-sectional area ($A$) and frontal perimeter ($p$).

Table 1 outlines the boundary conditions applied in the computational method using the Fluent 6.3.26 application for the aerodynamic analysis of the tandem minibus. The working fluid in this simulation is air with a density of 1.164 kg/m³ and a viscosity of 0.00001872 kg/m.s. The boundary conditions include a velocity inlet to regulate the flow velocity at the inlet, a pressure outlet at the exit as a pressure limit, and the surface of the minibus and the simulation domain configured as a wall. Simulations were conducted with airflow velocity variations of 8, 10, 12, 14, 16, 18, and 20 m/s to evaluate the effect of velocity changes on the flow characteristics around the tandem minibus.

Table 1 Boundary conditions for computational methods on tandem-aisled minibus

| | | |
|---|---|---|
| Fluid (air) properties | Density | 1.164 kg/m$^3$ |
| | Viscosity | 0.00001872 kg/m.s |
| Tandem minibus boundary conditions | Tandem minibus | Wall |
| | Inlet | Velocity inlet |
| | Outlet | Pressure outlet |
| | Wall | Wall |
| Upstream velocity | | 8, 10, 12, 14, 16, 18, and 20 m/s |

The pressure coefficient ($C_P$) and can be obtained by

$$C_P = \frac{h_{sm} - h}{h_{sm} - h_{tm}} \tag{3}$$

Eq. (3) involves variables and parameters such as the fluid flow (air) head at the test point on the object's surface ($h$), the static fluid flow (air) head in the manometer ($h_{sm}$), and the stagnation fluid flow (air) head in the manometer ($h_{tm}$). Meanwhile, the pressure conditions at room temperature in the research setting become the determining factor of the kinematic viscosity value of the fluid (air).

## 3. Result and Discussion

From this research, the results are obtained through both the experimental approach and the computational approach using the CFD program The applied fluid flow velocity was 8, 10, 12, 14, 16, 18, and 20 m/s for each distance to diameter ratio ($L/D$) of 0.227, 0.455, 0.682, 0.909, and 1.136. The data of this research is presented in the form of graph contours, including pressure contours, velocity contours, and vorticity contours.

The attached graphs exhibit the relationship of the pressure coefficient ($C_P$) with each position of the pressure tap ($T_P$) around the minibus for each level of variation of the ratio $L/D$ = 0.227, 0.455, 0.682, 0.909, and 1.136 are presented in Fig. 3. For Figs. 4-8, the attached graphs display the relationship of $C_P$ with each position of $T_P$ around the minibus at seven levels of Reynolds number variations (21891, 27363, 32836, 38308, 43781, 49254, and 54726). Meanwhile, the results of computational data using Fluent 6.3.26 include pressure contours, velocity contours, and vorticity contours at $L/D$ = 0.227, 0.455, 0.682, 0.909, and 1.136 for a speed of 20 m/s (Re = 54726) are shown in Figs. 9-13.

The variation of speed and $L/D$ ratio applied to the tandem minibus can affect the change of pressure coefficient at each point around the tandem minibus. This can delay the occurrence of airflow separation on the rear side of the minibus or prevent early flow separation on the tandem minibus surface.

When the tandem minibus is at the closest L/D ratio (0.227), the $C_P$ value increases, but when the $L/D$ ratio is increased to 0.455, the $C_P$ value stabilizes for both minibuses. Further increasing the $L/D$ ratio variation from 0.682 to 1.136 allows the rear-positioned minibus to experience free airflow, reducing the pressure influence of minibus 1.

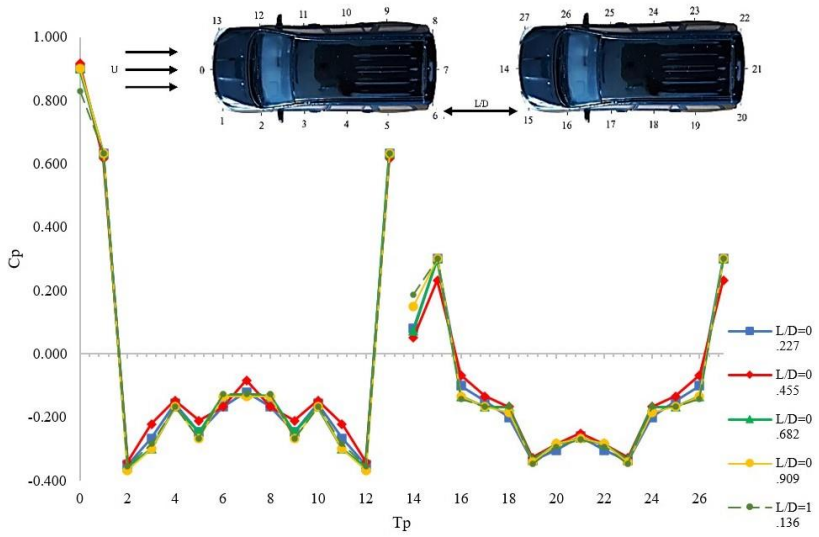


Fig. 3 Pressure coefficient ($C_P$) against pressure tap ($T_P$) for minibus 1 and 2 at condition $Re$ = 54726

Fig. 3 demonstrates the results of $C_P$ against each $T_P$ position around the minibus at five levels of variation $L/D$ = 0.227, 0.455, 0.682, 0.909, and 1.136 for $Re$ = 54726, showing a high-intensity $C_P$ increase occurs at $T_P$ 0, which is at the front position of minibus 1 and $T_P$ 14, at the front position of minibus 2. Then, there is a drastic decrease in $C_P$ at $T_P$ 2 - $T_P$ 12 minibus 1 and $T_P$ 16 - $T_P$ 26 minibus 2 at all levels of $L/D$ variation. This indicates that the $L/D$ variation affects the $C_P$ value at each point on the minibus wall surface, but at a ratio of $L/D$ = 0.227, the flow separation in tandemly arranged minibus is more effectively delayed.

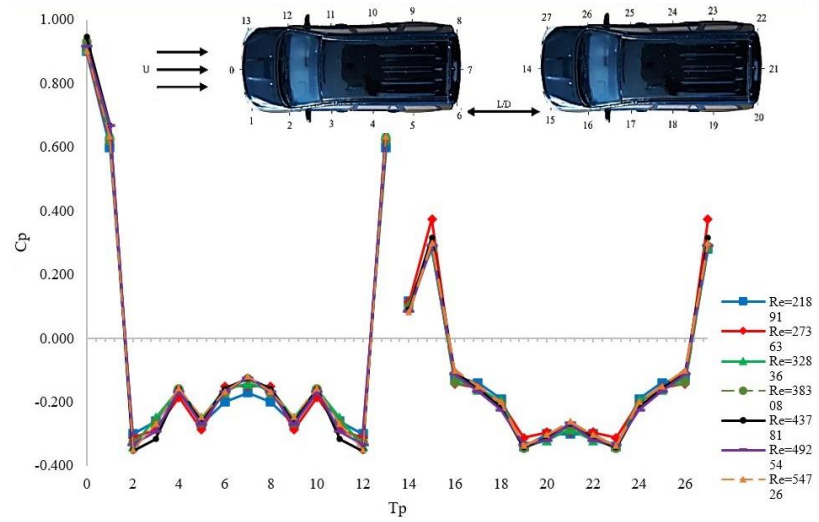


Fig. 4 Pressure coefficient ($C_P$) against pressure tap ($T_P$) for minibus 1 and 2 at condition $L/D$ = 0.227

Fig. 4 presents the $C_P$ results at each $T_P$ position around the tandem minibus at seven Reynolds number variations (21891, 27363, 32836, 38308, 43781, 49254, and 54726) for $L/D$ = 0.227. In this graph, it can be observed that a significant $C_P$ increase at $T_P$ 0 (front of minibus 1) and $T_P$ 14 (front of minibus 2). After that, there is a drastic decrease in $C_P$ values in the range of $T_P$ 2 to 12 in minibus 1, as well as at $T_P$ 16 to 26 in minibus 2 across all Reynolds numbers. This denotes that Reynolds affects $C_P$, especially in the front and rear areas of the vehicle. However, at higher Reynolds numbers, the changes in pressure distribution tend to be smaller.

Fig. 5 illustrates the $C_P$ results at each $T_P$ position around the tandem minibus at seven levels of Reynolds number variation (21891, 27363, 32836, 38308, 43781, 49254, and 54726) for a ratio of $L/D$ = 0.455. In this graph, it can be seen that a significant increase in $C_P$ occurs at $T_P$ 0, and $T_P$ 14. Following this, there is a drastic decrease in the $C_P$ value from $T_P$ 2 to $T_P$ 12 in the first minibus, as well as at $T_P$ 16 to $T_P$ 26 in the second minibus, for all variations of Reynolds number. This demonstrates that

the Reynolds number influences $C_P$, particularly in the front and rear areas of the vehicle, but at higher Reynolds numbers, the changes in pressure distribution tend to lessen.

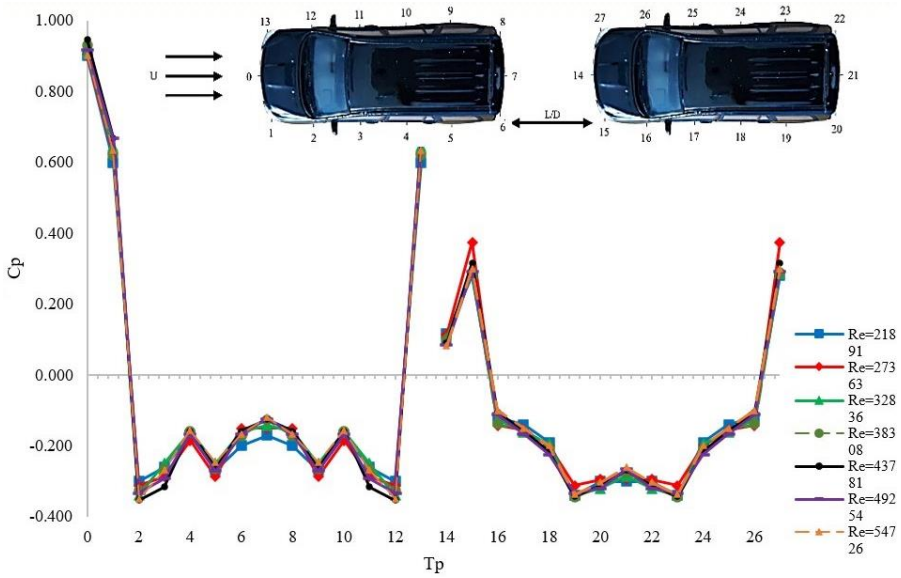


Fig. 5 Pressure coefficient ($C_P$) against pressure tap ($T_P$) for minibus 1 and 2 at condition $L/D$ = 0.455

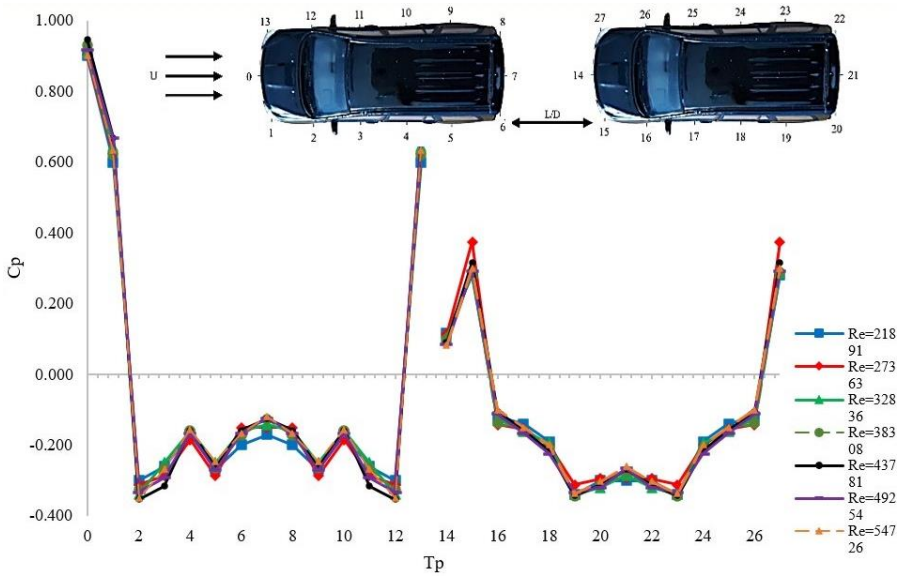


Fig. 6 Pressure coefficient ($C_P$) against pressure tap ($T_P$) for minibus 1 and 2 at condition $L/D$ = 0.682

Fig. 6 shows the $C_p$ distribution at each $T_P$ position around the tandem minibus for seven variations of Reynolds number (21891, 27363, 32836, 38308, 43781, 49254, and 54726) with a ratio of $L/D$ = 0.455. This graph shows a significant increase in $C_p$ occurs at $T_P$ 0, and $T_P$ 14. Thereafter, the $C_p$ values decrease significantly in the range of $T_P$ 2 to $T_P$ 12 for the first minibus, as well as in the range of $T_P$ 16 to $T_P$ 26 for the second minibus, applicable to all levels of Reynolds number variation. This indicates that the Reynolds number affects the $C_p$ distribution, especially in the front and rear areas of the vehicle, but at higher Reynolds numbers, the change in pressure distribution is relatively smaller.

Fig. 7 displays the $C_P$ distribution at each $T_P$ position around the tandemly arranged minibus at seven different Reynolds number levels (21891, 27363, 32836, 38308, 43781, 49254, and 54726) for a ratio of $L/D$ = 0.455. In this graph, it can be seen that a significant increase in $C_p$ occurs at $T_P$ 0, and $T_P$ 14. After that, the $C_p$ value decreases sharply from $T_P$ 2 to $T_P$ 12 for the first minibus, and from $T_P$ 16 to $T_P$ 26 for the second minibus, for all levels of Reynolds number variation. This shows that the Reynolds number affects the $C_p$ distribution, especially in the front and rear areas of the vehicle, whereas the changes in pressure distribution tend to be smaller at higher Reynolds numbers.

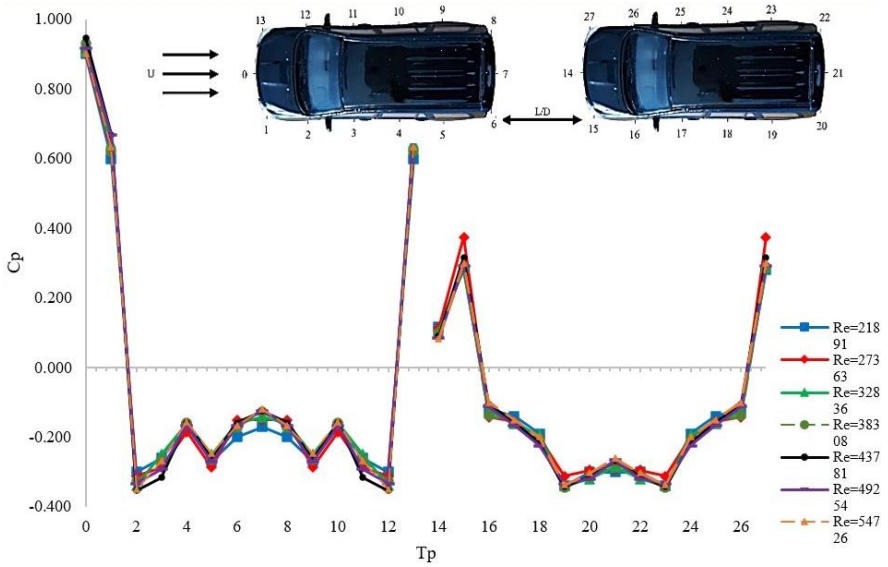


Fig. 7 Pressure coefficient ($C_P$) against pressure tap ($T_P$) for minibus 1 and 2 at condition $L/D$ = 0.909

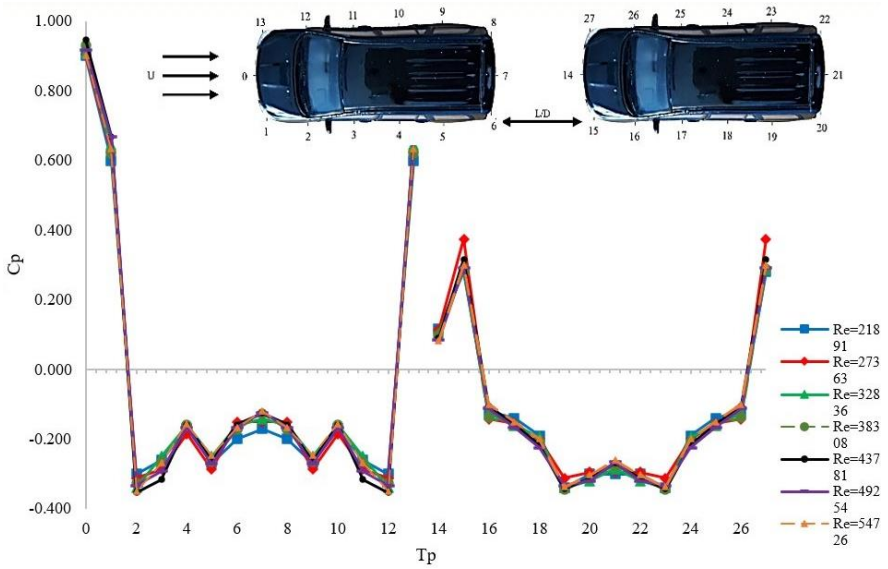


Fig. 8 Pressure coefficient ($C_P$) against pressure tap ($T_P$) for minibus 1 and 2 at condition $L/D$ = 1.136

Meanwhile, Fig. 8 presents the $C_P$ distribution at each $T_P$ point of the tandemly arranged minibus at seven variations of Reynolds numbers (21891, 27363, 32836, 38308, 43781, 49254, and 54726) with a ratio of $L/D$ = 0.455. From this graph, it can be seen that a significant increase in $C_P$ occurs at $T_P$ 0, and $T_P$ 14. Thereafter, the $C_P$ value drops dramatically between $T_P$ 2 and $T_P$ 12 for the first minibus, and between $T_P$ 16 and $T_P$ 26 for the second minibus, with this pattern prevailing for all levels of Reynolds number variation. These findings indicate that the Reynolds number affects the coefficient of pressure ($C_P$) on all sides of the minibus, but at higher Reynolds values, the changes in pressure distribution tend to lessen.

Table 2 presents the minimum pressure coefficient ($C_P$) values at $T_P$ 7 for minibus 1 and $T_P$ 21 for minibus 2 with $L/D$ = 0.227, 0.455, 0.682, 0.909, and 1.136, respectively. The results from Table 1 display that the minimum pressure coefficient that occurs in the tandem minibus series configuration is at $L/D$ = 0.455, with a value of $C_P$ = -0.083 for minibus 1 and $C_P$ = -0.250 for minibus 2. These minimum pressure coefficients are observed at $T_P$ 7 for minibus 1 and $T_P$ 21 for minibus 2 when the flow velocity is $U = 20$ m/s ($Re = 54726$).

Based on the attached Figs. 3-8, in general, the same characteristic pattern is produced in each variation of $L/D$ ratio and Reynolds number ($Re$) namely, flow separation consistently occurs between $T_P$ 2 and $T_P$ 13 for minibus 1 and between $T_P$ 16 and $T_P$ 26 for minibus 2. However, more delayed flow separation occurs in tandemly arranged minibuses at a variation ratio of $L/D$ = 0.227. This indicates that at this ratio, the fluid flow conditions are more stable and controlled.

Table 2 Minimum pressure coefficient for tandem minibus at $T_P$ 7 and $T_P$ 21

| L/D | *Minibus 1 (M1)* | *Minibus 2 (M2)* |
|---|---|---|
| 0.227 | -0.120 | -0.260 |
| 0.455 | -0.083 | -0.250 |
| 0.682 | -0.127 | -0.265 |
| 0.909 | -0.133 | -0.267 |
| 1.136 | -0.127 | -0.270 |

Figs. 9-13 display the simulation results from the top perspective of the tandem minibus model, with five levels of variation (*L/D* = 0.227, 0.455, 0.692, 0.909, and 1.136) at a constant flow velocity of 20 m/s (*Re* = 54726) for each contour. Fig. 9 displays the results for the (a) pressure contours, (b) velocity magnitude contours, and (c) vorticity contours. These results were obtained using the computational method with the Fluent 6.3.26 application. These computational simulation results were validated with the experimental data listed in Fig. 3, which illustrates the occurrence of the flow separation phenomenon in the tandem minibus model.

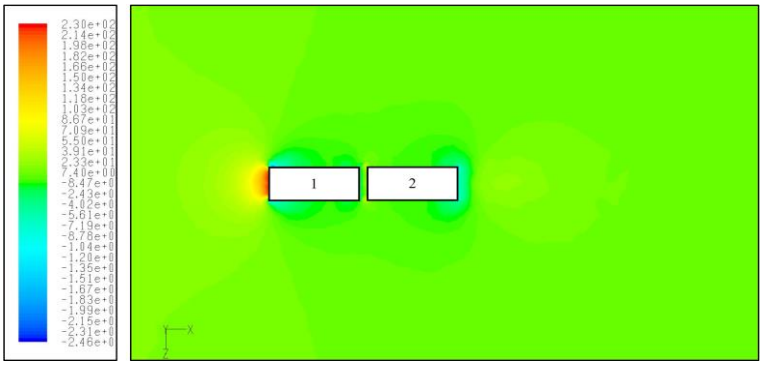


(a) Pressure contour

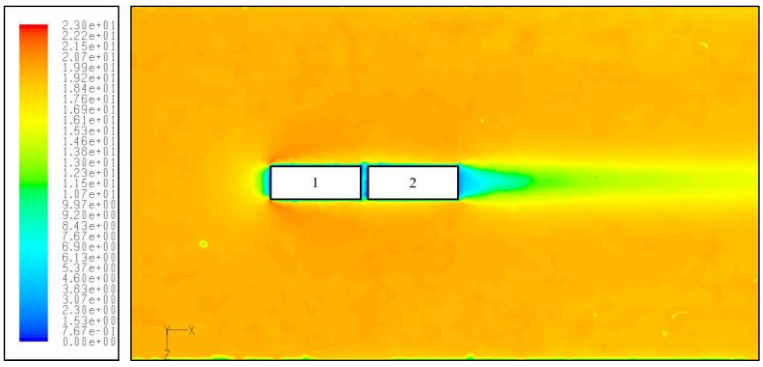


(b) Velocity contour

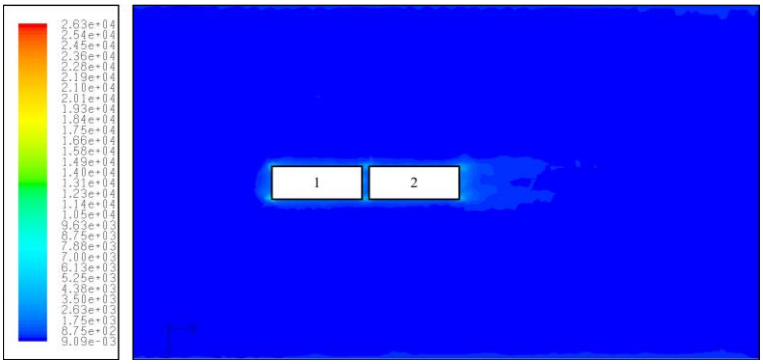


(c) Vorticity contour

Fig. 9 The CFD simulation results at a flow rate of *U* = 20 m/s (Re = 54726), with *L/D* = 0.277 arranged in tandem

Fig. 9(a) presents a tandem minibus model with increasing pressure at the front of minibus 1, which then experiences a significant decrease in the left, right, and rear sides of minibus 1. For minibus 2, the pressure at the front remains balanced without significant fluctuations, indicating stability in these conditions. A decrease in pressure is also observed at the left, right, and rear sides of minibus 2. Fig. 9(b) shows that there is a slight flow separation phenomenon that can be observed between the positions of minibus 1 and 2. Fig. 9(c) also indicates the presence of small eddies or vortices in the rear area of both minibuses.

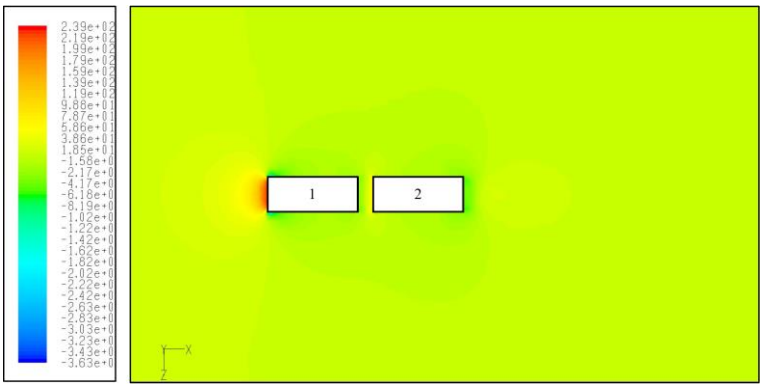


(a) Pressure contour

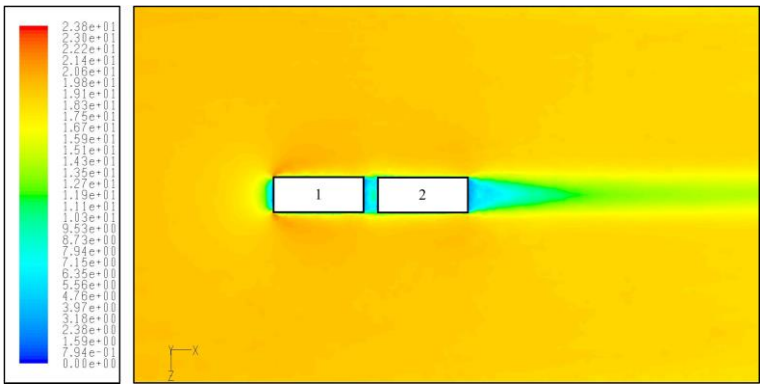


(b) Velocity contour

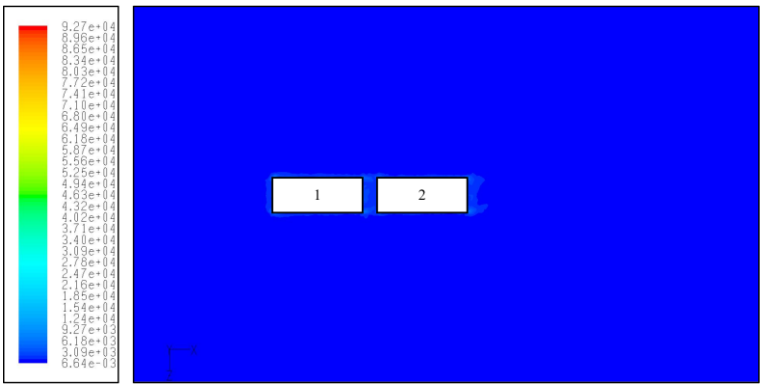


(c) Vorticity contour

Fig. 10 The CFD simulation results at a flow rate of $U$ = 20 m/s (Re = 54726), with $L/D$ = 0.455 arranged in tandem

Fig. 10(a) displays conditions for increased pressure in the front of minibus 1, after which it experiences a significant decrease in the left, right, and rear sections of minibus 1. At the same time, for minibus 2, the pressure at the front displays the balance results. There is no significant fluctuation since the front is stable. Subsequently, the left, right, and rear sections of minibus 2 also experienced a significant decrease in pressure. Meanwhile, Fig. 10 (b) shows the phenomenon of small flow separation in both minibuses. In the case of Fig. 10(c) indicates the presence of a relatively small vorticity located right at the rear of both minibuses.

Furthermore, in Fig. 11(a), there is a significant increase in pressure at the front of minibus 1, followed by a significant decrease in pressure in the left, right, and rear areas of the minibus. Meanwhile, for minibus 2, the front exhibits stability or no significant fluctuations, but there is a considerable decrease in pressure in the left, right, and rear areas of minibus 2. Fig. 11(b) depicts a small-scale phenomenon of flow separation between the two minibuses. Additionally, in Fig. 11(c), this also leads to a significant vorticity phenomenon at the rear of both minibuses when compared to the phenomenon observed in Fig. 10(c).

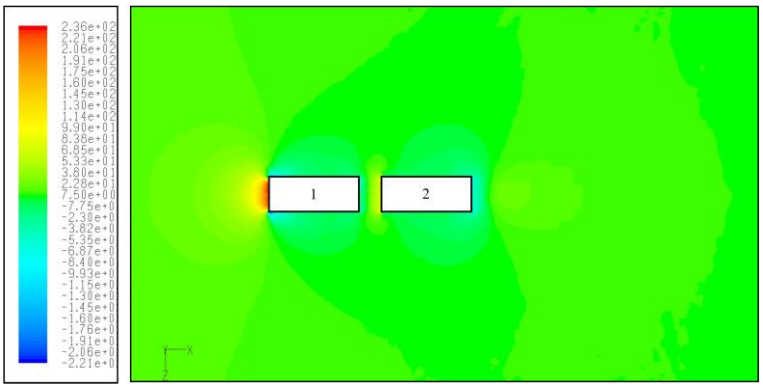


(a) Pressure contour

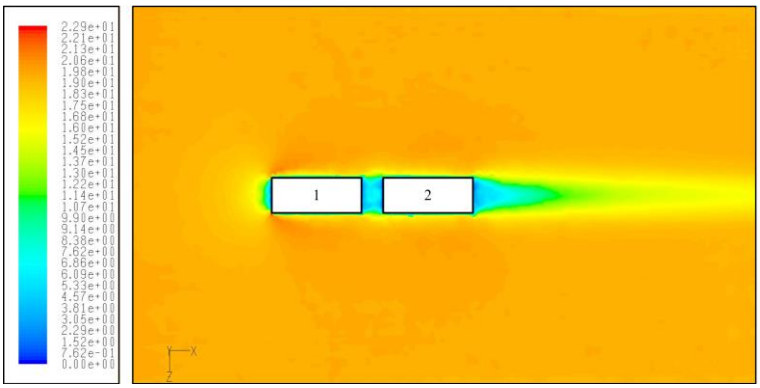


(b) Velocity contour

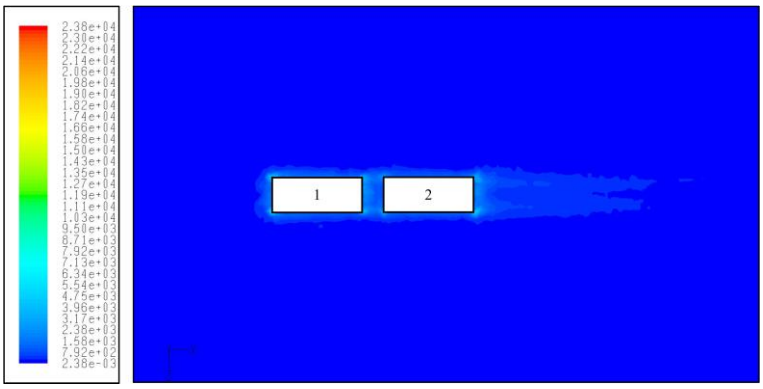


(c) Vorticity contour

Fig. 11 The CFD simulation results at a flow rate of $U$ = 20 m/s (Re = 54726), with $L/D$ = 0.682 arranged in tandem

Fig. 12(a) illustrates an increase in pressure at the front of minibus 1 followed by a significant decrease in pressure at its left, right, and rear sides, while on the other hand, minibus 2 depicts stability at its front with minimal significant fluctuations, while its left, right, and rear sides experience a considerable decrease in pressure. On the other hand, Fig. 12(b) illustrates a phenomenon where small-scale separated flow occurs between the two minibusses. In the context of Fig. 12(c), it can be observed that there is a significant vorticity phenomenon at the rear of both minibuses, indicating a substantial disturbance at the rear of both test objects.

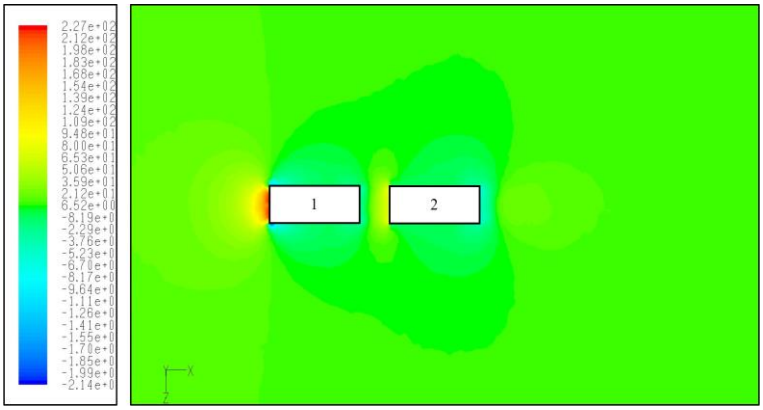


(a) Pressure contour

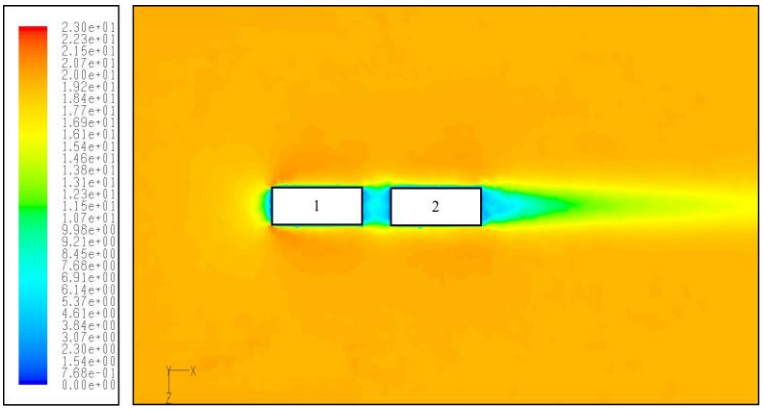


(b) Velocity contour

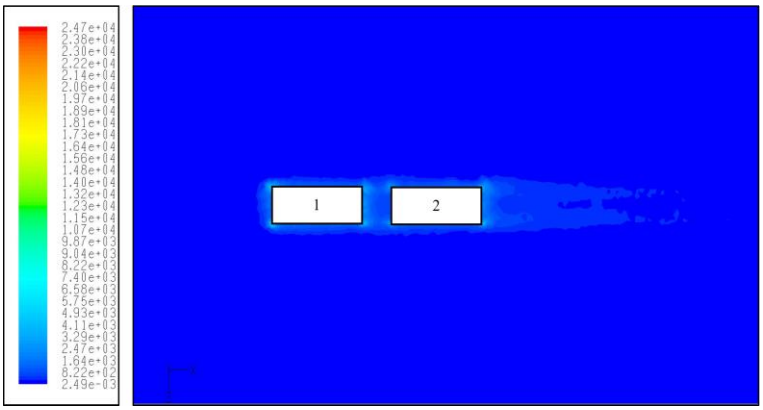


(c) Vorticity contour

Fig. 12 The CFD simulation results at a flow rate of $U$ = 20 m/s (Re = 54726), with $L/D$ = 0.909 arranged in tandem

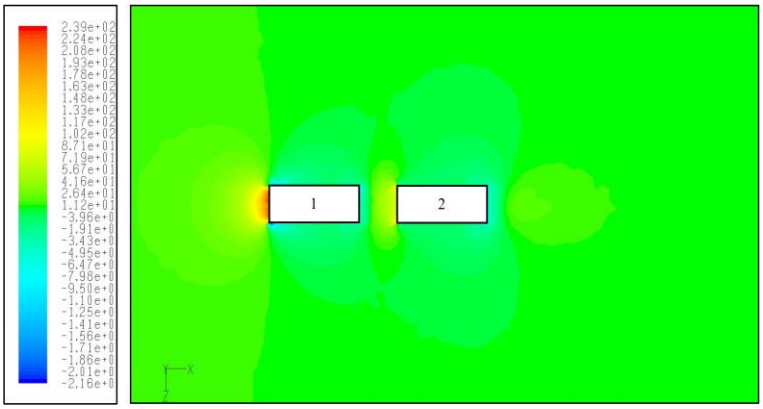


(a) Pressure contour

Fig. 13 The CFD simulation results at a flow rate of $U$ = 20 m/s (Re = 54726), with $L/D$ = 1.136 arranged in tandem

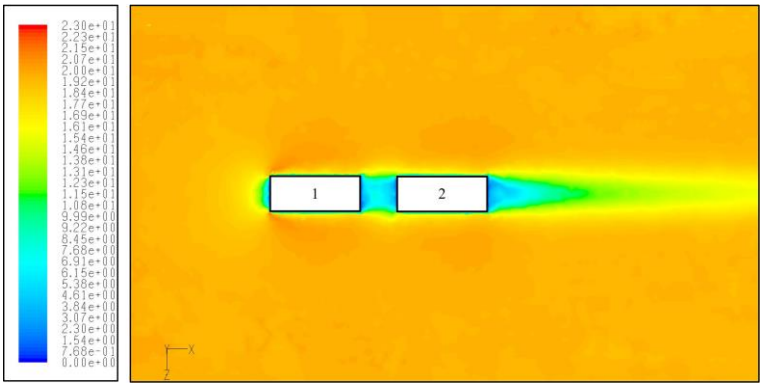


(b) Velocity contour

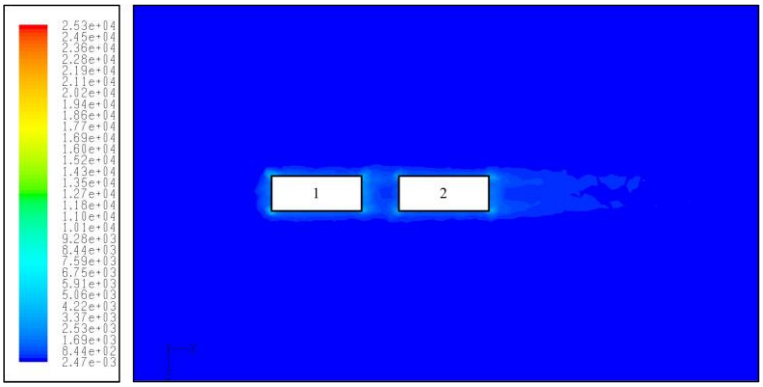


(c) Vorticity contour

Fig. 13 The CFD simulation results at a flow rate of $U$ = 20 m/s (Re = 54726), with $L/D$ = 1.136 arranged in tandem(continued)

Next, Fig. 13(a) describes that there is an increase in pressure on the front of minibus 1, while the front of minibus 2 appears to be stable with no significant fluctuation. This is followed by a fairly intense pressure drop fluctuation caused by both the left and right minibus, accompanied by the ensuing high-pressure drop at the rear. Meanwhile, Fig. 13(b) illustrates a phenomenon where separate flows occur on a small scale between the two test objects. Fig. 13(c) displays the phenomenon of significant vorticity occurring at the rear of both minibuses.

## 4. Conclusions

This study analyzes the aerodynamic characteristics of two minibuses arranged in a tandem configuration using experimental and computational methods. The tests were conducted in a subsonic wind tunnel with a 1:40-scale minibus model equipped with 14 pressure taps. Experimental data were compared with numerical simulation results using Fluent 6.3.26 software to obtain pressure, velocity, and vorticity distributions. The main focus of the study was to identify the effects of varying the spacing between minibus on flow separation and pressure distribution.

(1) The optimum spacing in a tandem configuration was found at $L/D$ = 0.455, where smaller flow separation occurs, resulting in a more stable pressure distribution around the minibus. This suggests that choosing the right spacing can minimize aerodynamic drag, ultimately improving the airflow efficiency around the minibus.

(2) Better aerodynamic efficiency improves minibus performance, especially in terms of stability and potential reductions in energy consumption. This configuration can reduce drag and improve minibus fuel efficiency under real conditions by suppressing flow separation and dominant negative $C_P$ values. This study also shows the importance of exploring other parameters, such as minibus shape, model scale, and crosswind effects, to better understand aerodynamic performance in real-world applications.

## Nomenclature

| | |
|---|---|
| A | Frontal cross-sectional area |
| $C_p$ | Pressure coefficient |
| D | Hydraulic diameter |
| h | Head of airflow in the manometer |
| $h_{sm}$ | Head of static airflow in the manometer |
| $h_{tm}$ | Head of a stagnation airflow in the manometer |
| L | Tandem minibus distance |
| p | Frontal perimeter |
| Re | Reynolds number |
| U | Inlet airspeed to the wind tunnel |
| ρ | Air density |
| υ | The kinematic velocity of air |

## Conflicts of Interest

The authors declare no conflict of interest.

## References

[1] N. Salam, R. Tarakka, Jalaluddin, M. A. Jimran, and M. Ihsan, "Flow Separation in Four Configurations of Three Tandem Minibus Models," International Journal of Mechanical Engineering and Robotics Research, vol. 10. no. 5, pp. 236-247, 2021.

[2] H. Kepekçi, "Investigation of the Effect of the Use of Top Deflectors on Aerodynamic Performance in Vehicles with CFD Analysis," International Journal of Automotive Engineering and Technologies, vol. 12, no. 2, pp. 44-50, 2023.

[3] D. Kumar, K. Sourav, and S. Sen, "Steady Separated Flow Around a Pair of Identical Square Cylinders in Tandem Array at Low Reynolds Numbers," Computer & Fluids, vol. 191, article no. 104244, 2019.

[4] Z. ul-Islam, S. ul-Islam, and C. Y. Zhou, "The Wake and Force Statistics of Flow Past Tandem Rectangles," Ocean Engineering, vol. 236, article no. 109476, 2021.

[5] G. Chen, X. F. Liang, D. Zhou, X. B. Li, and F. S. Lien, "Numerical Study of Flow and Noise Predictions for Tandem Cylinders Using Incompressible Improved Delayed Detached Eddy Simulation Combined with Acoustic Perturbation Equations," Ocean Engineering, vol. 224, article no. 108740, 2021.

[6] D. Zhang, D. Liang, J. Deng, Y. Liu, and J. Xie, "On the Spanwise Periodicity within the Gap Between Two Different-Sized Tandem Circular Cylinders at Re = 3900," Journal of Marine Science and Engineering, vol. 12, no. 6, article no. 866, 2024.

[7] M. R. Rastan and M. M. Alam, "Transition of Wake Flows Past Two Circular or Square Cylinders in Tandem," Physics of Fluids, vol. 33, no. 8, article no. 081705, 2021.

[8] P. G. de Moraes and L. A. A. Pereira, "Surface Roughness Effects on Flows Past Two Circular Cylinders in Tandem Arrangement at Co-Shedding Regime," Energies, vol. 14, no. 24, article no. 8237, 2021.

[9] R. Dubois and T. Andrianne, "Flow Around Tandem Rough Cylinders: Effects of Spacing and Flow Regimes," Journal of Fluids and Structures, vol. 109, article no. 103465, 2022.

[10] N. Salam, I. N. G. Wardana, S. Wahyudi, and D. Widhiyanuriyawan, "Fluid Flow Through Triangular and Square Cylinders," Australian Journal of Basic and Applied Sciences, vol. 8, no. 2, pp. 193-200, 2014.

[11] A. Etminan, M. Moosavi, and N. Ghaedsharafi, "Characteristics of Aerodynamics Forces Acting on Two Square Cylinders in the Streamwise Direction and Its Wake Patterns," Proceedings of European Conference of Chemical Engineering, and European Conference of Civil Engineering, and European Conference of Mechanical Engineering, and European Conference of Control, pp. 209-217, 2010.

[12] N. Salam, R. Tarakka, Jalaluddin, M. Ihsan, and M. A. Jimran, "Flow Drags Across Three Minibus Car Models Arranged in Tandem in Four Configurations," IOP Conference Series: Materials Science and Engineering, vol. 1173, article no. 012046, 2021.

[13] R. Maryami, S. A. S. Ali, M. Azarpeyvand, A. A. Dehghan, and A. Afshari, "The Influence of Cylinders in Tandem Arrangement on Unsteady Aerodynamic Loads," Experimental Thermal and Fluid Science, vol. 139, article no. 110709, 2022.

[14] S. Ahmad, Shams-ul-Islam, H. Waqas, D. Liu, T. Muhammad, I. Khan, et al., "Flow Transition and Fluid Forces Reduction for Flow Around Two Tandem Cylinders," Results in Physics, vol. 51, article no. 106681, 2023.

[15] X. Du, Q. Xu, H. Dong, and L. Chen, "Physical Mechanisms behind the Extreme Wind Pressures on Two Tandem Square Cylinders," Journal of Wind Engineering and Industrial Aerodynamics, vol. 231, article no. 105249, 2022.

[16] H. Abdul-Rahman, H. Moria, and M. R. Rasani, "Aerodynamic Study of Three Cars in Tandem Using Computational Fluid Dynamics," Journal of Mechanical Engineering and Sciences, vol. 15, no. 3, pp. 8228-8240, 2021.

[17] A. H. Rabiee, F. Rafieian, and A. Mosavi, "Active Vibration Control of Tandem Square Cylinders for Three Different Phenomena: Vortex-Induced Vibration, Galloping, and Wake-Induced Vibration," Alexandria Engineering Journal, vol. 61, no. 12, pp. 12019-12037, 2022.

[18] P. Sikdar, S. M. Dash, K. P. Sinhamahapatra, and A. Sharma, "Splitter Plate-Based Flow Control Study for Two Square Cylinders in Tandem Arrangement," Ocean Engineering, vol. 281, article no. 115022, 2023.

[19] R. Radovic, F. Salehi, and S. Diasinos, "A Detailed Numerical Study on Aerodynamic Interactions of Tandem Wheels on a Generic Vehicle," Fluids, vol. 8, no. 10, article no. 281, 2023.

[20] Q. Zhang, R. Xue, and H. Li, "Aerodynamic Exploration for Tandem Wings with Smooth or Corrugated Surfaces at Low Reynolds Number," Aerospace, vol. 10, no. 5, article no. 427, 2023.

[21] N. Salam, R. Tarakka, J. Jalaluddin, and R. Bachmid, "The Effect of the Addition of Inlet Disturbance Body (IDB) to Flow Resistance Through the Square Cylinders Arranged in Tandem," International Review of Mechanical Engineering, vol. 11, no. 3, pp. 181-190, 2017.

[22] H. Zhu, J. Zhong, Z. Shao, T. Zhou, and M. M. Alam, "Fluid-Structure Interaction Among Three Tandem Circular Cylinders Oscillating Transversely at a Low Reynolds Number of 150," Journal of Fluids and Structures, vol. 130, article no. 104204, 2024.

[23] T. Liu, L. Zhou, D. Huang, H. Zhang, and C. Wei, "Aspect Ratio and Interference Effects on Flow Over Two Rectangular Cylinders in Tandem Arrangement," Ocean Engineering, vol. 271, article no. 113731, 2023.

[24] Y. A. Cengel and J. M. Cimbala, Fluid Mechanics Fundamentals and Applications, 3rd ed., New York: McGraw-Hill Companies, 2014.